ABSTRACT

Discovery of a Novel Adenosine 5’-phosphosulfate (APS) Reductase from the Methanarcheon *Methanocaldococcus jannaschii*

Jong-Sun Lee, M.S.

Mentor: Sung-Kun Kim, Ph.D.

This thesis presents the first discovery of adenosine 5'-phosphosulfate reductase (APR), a key enzyme of the sulfate reduction pathway, in the methanarchaeon *Methanocaldococcus jannaschii*. While the sulfate reduction pathway is present in other organisms, it is not expected to exist in methanarchaea because their habitats often already possess an abundance of reduced sulfur, particularly H_2S. However, the gene product of open reading frame (ORF) *Mj0973* in *M. jannaschii* possesses sequence similarities with known APRs and 3’-phosphoadenosine-5’-phosphosulfate reductases (PAPRs) from various organisms. In order to further investigate this ORF, the gene *Mj0973* from *M. jannaschii* was expressed and the resulting protein was purified. Kinetic studies revealed that the purified protein is able to reduce APS with *E. coli* thioredoxin (Trx) supplied as the electron donor, but is unable to reduce PAPS. The apparent K_m, V_{max}, and k_{cat}/K_m values at pH 8.0 and 30 ^oC were 0.29 μM, 0.079μMmg^{-1}min^{-1}, and 299,655 M^{-1}s^{-1}, respectively. This observation of APR activity strongly indicates the presence of an APS-utilizing sulfate reduction pathway in the methanarchaeon *M. jannaschii.*

Discovery of a Novel Adenosine 5'-phosphosulfate (APS) Reductase from the Methanarcheon *Methanocaldococcus jannaschii*

by

Jong-Sun Lee, B.S.

A Thesis

Approved by the Department of Chemistry and Biochemistry

_____

Patrick J. Farmer, Ph.D. Chairperson

Submitted to the Graduate Faculty of
Baylor University in Partial Fulfillment of the
Requirements for the Degree
of
Master of Science

Approved by the Thesis Committee

_____

Sung-Kun Kim, Ph.D., Chairperson

_____

Mary Lynn Trawick, Ph.D.

_____

Sascha Usenko, Ph.D.

Accepted by the Graduate School
December 2010

_____

J. Larry Lyon, Ph.D., Dean

Page bearing signatures is kept on file in the Graduate School

TABLE OF CONTENTS

LIST OF FIGURES

LIST OF TABLES

LIST OF ABBREVIATIONS

APR – Adenosine 5’-phosphosulfate reductase

APS – Adenosine 5’-phosphosulfate

Asn – Asparagine

ATP – Adenosine triphosphate

AtAPR – *Arabidopsis thaliana* APR

BsAPR – *Bacillus subtilis* APR

Cys – Cysteine

DNA – Deoxyribonucleic acid

E. coli – *Escherichia coli*

EDTA – Ethylenediaminetetraacetic acid

Grx – Glutaredoxin

HEPES – 4-(2-hydroxyethyl)-1-piperazineethanesulfonic acid

IPTG – Isopropyl-beta-D-thiogalactopyranoside

LB – Luria broth

LPLC – Low pressure liquid chromatography

MES – 2-(*N*-morpholino)ethanesulfonic acid

Mj – *Methanocaldococcus jannaschii*

NADPH – Nicotinamide adenine dinucleotide phosphate

NCBI – National Center for Biotechnology Information

ORF – Open reading frame

PAGE – Polyacrylamide gel electrophoresis

PAPR – 3’-phosphoadenosine-5’-phosphosulfate reductase

PAPS – 3’-phosphoadenosine-5’-phosphosulfate

PCR – Polyacrylamide gel electrophoresis

PDB – Protein data bank

PpAPR – *Physcomitrella patens*

RMSD – Root mean square

SDS – Sodium dodecyl sulfate

Thr – Threonine

Trx – Thioredoxin

Tyr – Tyrosine

UV – Ultraviolet

VIS – Visible

ACKNOWLEDGMENTS

First of all, I would like to express the deepest appreciation to my family. This thesis would not have been possible without the support and love they have provided me throughout my entire life and particularly since my move to America. My parents, Dong-Il Lee and Min-Young Lee, who are the most important part of my life, have always believed in me no matter how far apart we were; the distance only matters to the mind, but not to the heart. You both really mean the world to me. To my brother, Joong-Won Lee, who is my only sibling and my best friend in my life, I always appreciate your unconditional love and encouragement.

I am heartily thankful to my mentor Dr. Sung-Kun Kim for giving me the opportunity of being part of his research group, for the guidance, the support, and the time that he dedicated to me. Without his expertise, understanding, patience, motivation and encouragement, I would not have considered a graduate career in Chemistry and Biochemistry research. I would also like to thank my committee members, Dr. Mary Lynn Trawick and Dr. Sascha Usenko, and Dr. Charles Garner, Dr. Sang-Chul Nam, and Dr. Paul Primrose for their encouragement and invaluable advice to complete this last requirement of my master program.

In addition, I am thankful to all the members of my group, past and present; Sheena Shipley, Deric Hagy, Taylor Foster, Mieke Lahousse, Sara Rae Schlesinger, Ethan White, Jenny Vu, Valerie Tapia, Connie Tang, and Kristin Brown. They cheer me up every time I was depressed and stressful and make my days in the lab enjoyable. Especially, I would like to express my gratitude to post-doctor of my group, Sang-Gon Kim, for teaching me research techniques and giving me life advice.

I am blessed to have my special friends, Jung-Hyun Kim, Dae-Hyun Kim, Dong-Ik Shin, Joseph Lee. Thanks for listening, for comforting me, for all of the advice, and for being there for me. I really appreciate your friendship and wish you all a bright future.

Lastly, special thanks to my lover, Juri Yamashita, for all the support and love. Thanks for always being there and showing me how much you care.

DEDICATION

To my grandparents and grand-uncle, without whose patience, understanding, support, and most of all love, the achievement of this work would not have been possible

CHAPTER ONE

Introduction

Sulfur is an important element that is used in all living organisms for various purposes. Since the major form of sulfur available in nature is sulfate [1], sulfate metabolism in organisms has been intensively studied. It has been found that bacteria, cyanobacteria, archaea, fungi and plants reduce sulfate to sulfide via a reduction pathway, typically with thioredoxin (Trx) or glutaredoxin (Grx) as electron donors [2, 3]. The first finding of the biosynthesis of the sulfate reductive pathway was in the bacteria Escherichia coli, in which sulfate is reduced to APS and then converted to PAPS. The outline is shown in Fig 1.

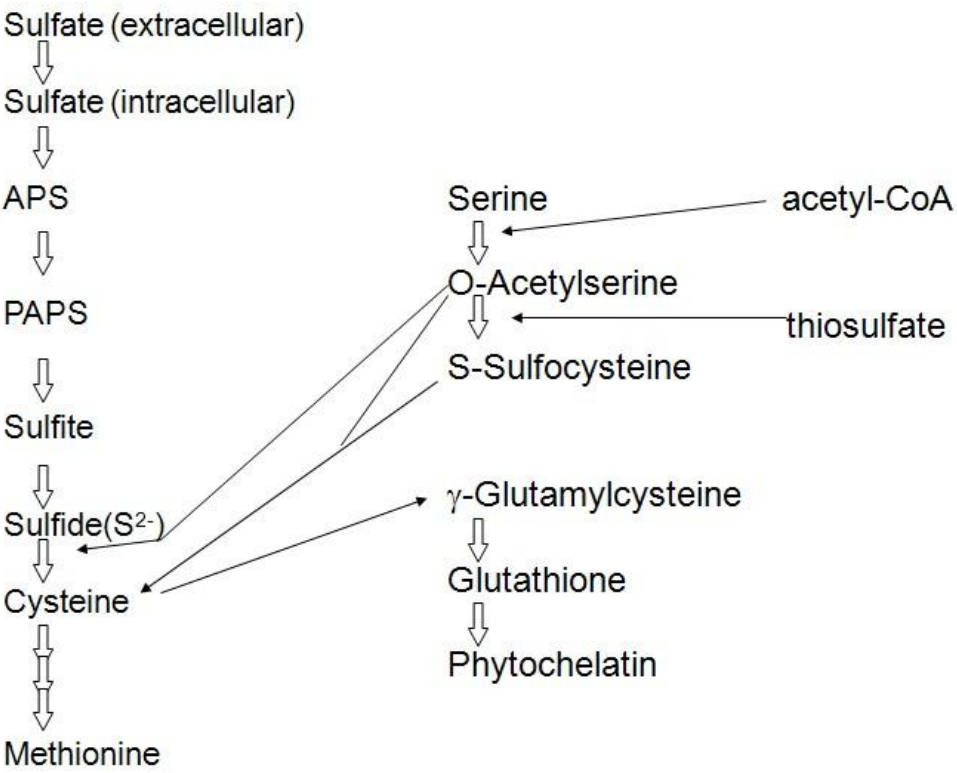

Figure 1. Biosynthesis of the sulfate reductive pathway in E. coli (modified from [31])

Later, the pathway was modified as outlined in Fig. 2, where sulfate is activated by ATP to form adenosine 5'-phosphosulfate (APS) and then APS can be reduced to sulfite by the catalysis of APS reductase.

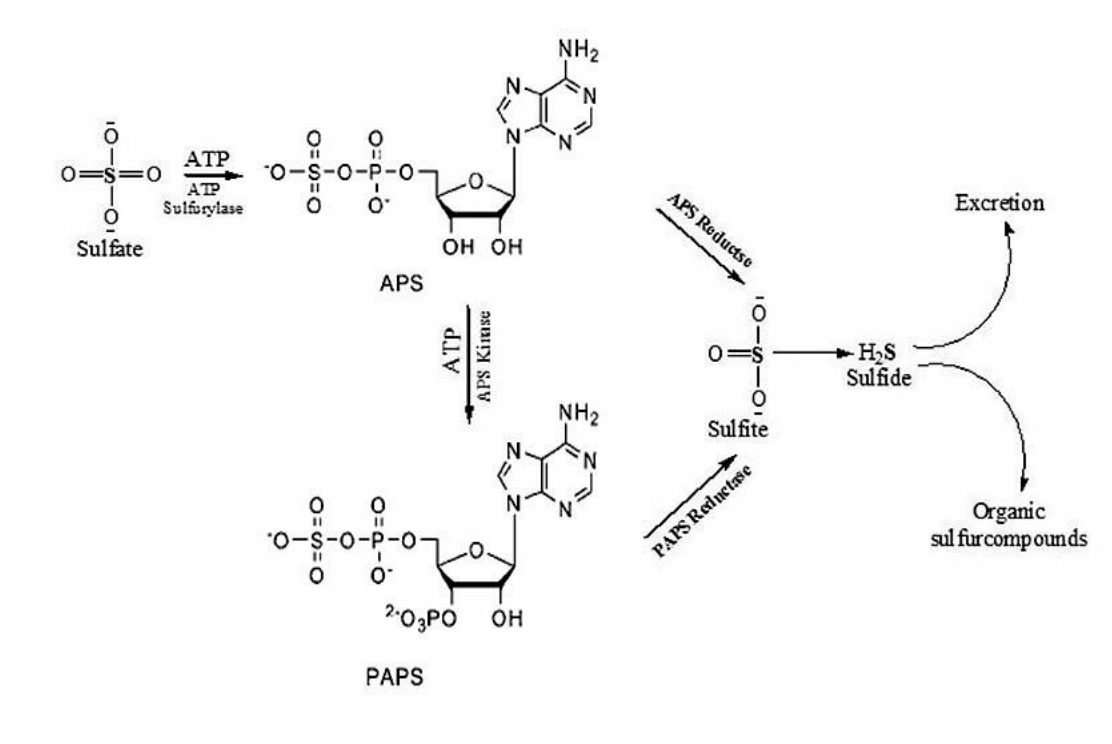

Figure 2. Sulfate reduction pathway. The chemical names or acronyms are indicated below or above the structure. Enzyme names are indicated below or above the arrows. (adopted from [2])

The activated sulfate can either be reduced directly to sulfite by APS reductase (APR) or can be phosphorylated to form an intermediate, 3'-phosphoadenosine-5'-phosphosulfate (PAPS), which is then reduced by PAPS reductase (PAPR) to sulfite. Sulfite is further reduced to hydrogen sulfide, which can either be incorporated into organic compounds (assimilation) or released as a waste product (dissimilation) [1, 2]. APR and PAPR are two key enzymes in this sulfate reduction pathway [4].

Methanocaldococcus jannaschii is a hyperthermophilic, methane-producing archaeon that resides near deep-sea hydrothermal vents (Fig. 3) [5].

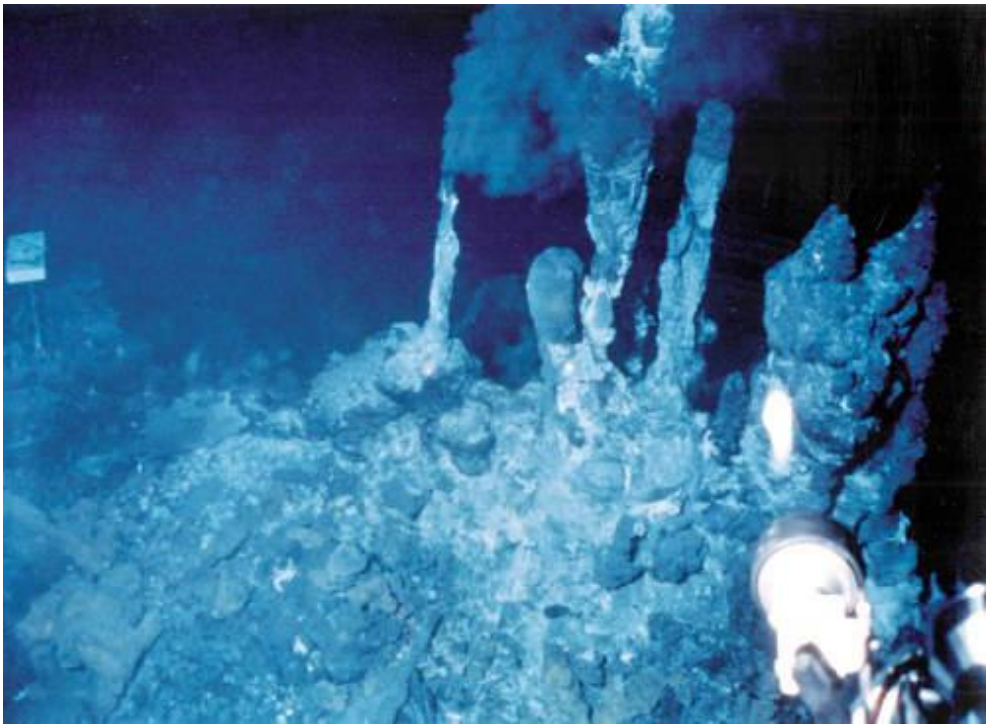

Figure 3. Hydrothermal vent where *Methanocaldococcus jannaschii* was found.
This figure is adopted from http://microbialgenomics.energy.gov/primer/tree.shtml.

The sulfate reduction pathway is expected to be absent in this species because the habitat of methanogens is typically rich in a reduced form of sulfur, H_2S [6, 7], making sulfate reduction unnecessary. Moreover, sulfite, an intermediate of the sulfate reduction pathway, is a known inhibitor of methanogenesis, a metabolically essential process in methanogens [5, 8]. Therefore, no effort has previously been made to examine *M. jannaschii* for the presence of APR or PAPR.

However, when the genome sequence of *M. jannaschii* was completely elucidated [9] open reading frame (ORF) *Mj0973* appeared to have some sequence similarities with APRs and PAPRs [5, 9]. The recent discovery of coenzyme F_{420} dependent sulfite reductase, an enzyme in *M. jannaschii* which catalyzes the reduction of sulfite to sulfide, also indicates the potential presence of the sulfate reduction pathway in this organism [5]. Motivated by the aforementioned studies, the protein expressed by ORF *Mj0973* was examined via homologous sequence analysis, *in silico*

docking and *in vitro* studies. As illustrated below, this study has resulted in the first discovery of APR in the methanarchaeon *M. jannaschii*, suggesting the possibility of an APS-utilizing sulfate reduction pathway in this organism.

CHAPTER TWO

Materials and methods

Bioinformatics

Sequence analysis was performed with BioEdit software. The protein sequences used for the analysis were obtained from NCBI sequence databases (http://www.ncbi.nlm.nih.gov/) as follows: APRs from plant (*Arabidopsis thaliana* APR1and 2 and *Catharanthus roseus*), green alga (*Enteromorpha intestinalis*) and bacteria (*Burkholderia cepacia, Pseudomonas aeruginosa, Mycobacterium tuberculosis and Bacillus subtilis*) and PAPRs from fungi (*Saccharomyces cerevisiae and Emericella nidulans*) yeast (*Schizosaccharomyces pombe*) and bacteria (*Thiocapsa roseopersicina, Salmonella typhimurium, Escherichia coli,* S*ynechococcus* and *Synechocystis*). Phylogenetic analysis was conducted on amino acid sequence alignment by ClustalW with BioEdit, and the neighbor-joining tree of the aligned amino acid sequences was generated by MEGA version 4.0 [10].

Computational Docking Simulations

The Dundee PRODRG[2] server was applied to generate a topological description of the substrates APS and PAPS (http://davapc1.bioch.dundee.ac.uk/programs/prodrg/prodrg.html) [11]. This server converted 2D compounds drawn by the JME molecular editor to 3D coordinates in PDB format, adding hydrogen atoms (Fig. 4).

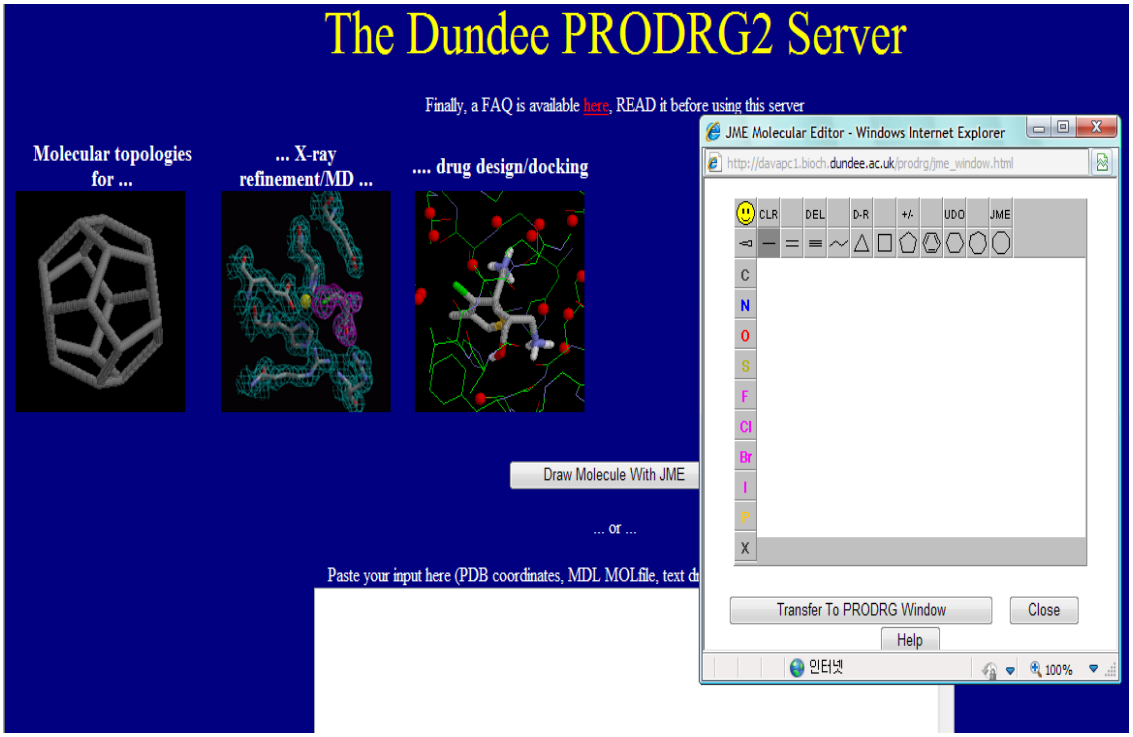

Figure 4. The Dundee PRODRG2 Server. This figure is adopted from http://davapc1.bioch.dundee.ac.uk/prodrg/

The 3D structures of the substrates, in PDB format, were then docked with a homology modeling-based structure of Mj0973 obtained from SWISS-MODEL, a web-based service accessible via the ExPASy server (http://swissmodel.expasy.org/workspace/index.php?func=modelling_overview) (Fig. 5) [12], using AutoDock4.0 (http://autodock.scripps.edu).

Cloning of Mj0973

The *Mj0973* coding sequence was amplified from *M. jannaschii* genomic DNA with GoTaq® DNA Polymerase (obtained from Promega) using the following PCR primers:

Forward: 5'-CACCATGGACGATAAATTTGCCTCTAAG-3'

Reverse: 5'-TTACTTTTTTTCTTTATTTTCTAATAT-3'

The four underlined nucleotides, CACC, base pair with the overhang sequence, GTGG,

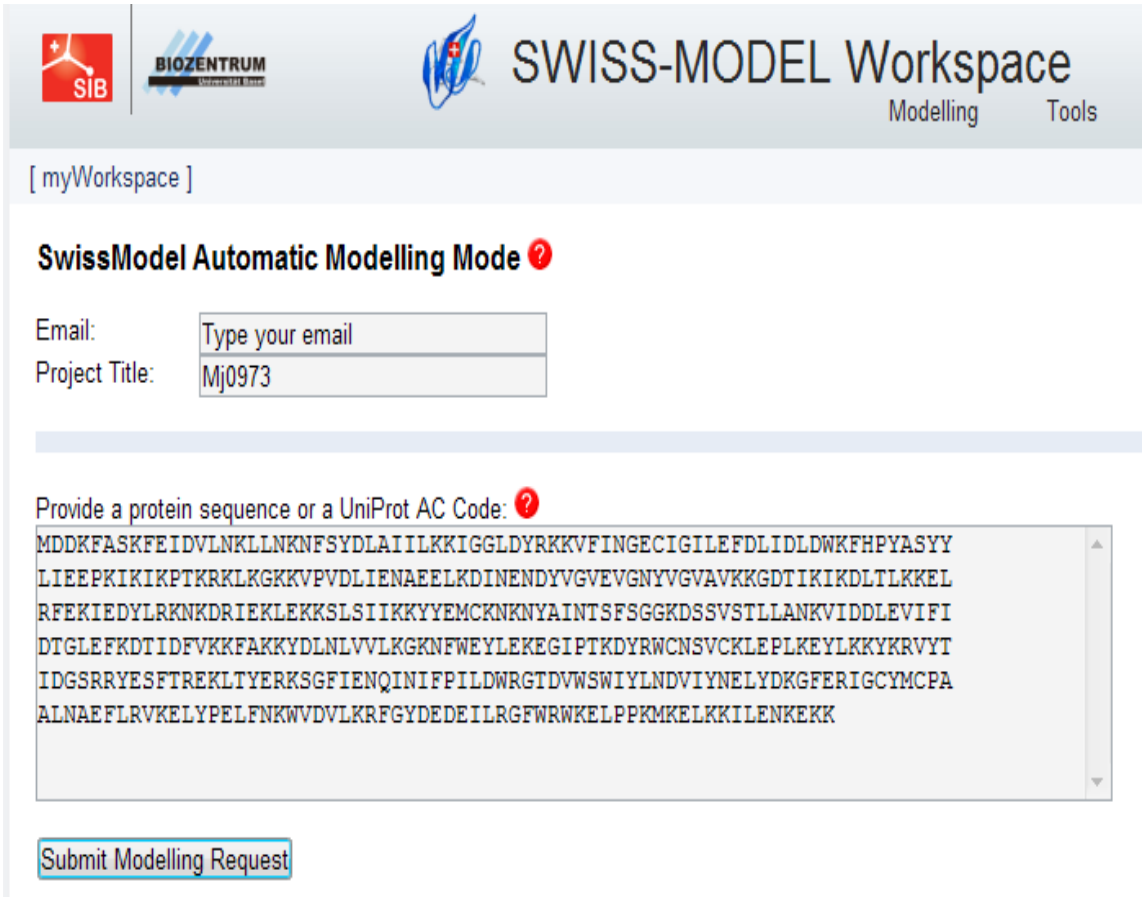

Figure 5. Swiss-Model building. Modelling requests are computed by the SWISS-MODEL server homology modelling pipeline. This figure is obtained from http://swissmodel.expasy.org/workspace/

in pET100 TOPO vector. This vector has a T7/lac promoter for highly efficient expression and a lac operator directly downstream for added regulation of basal expression. Using this vector for cloning, no ligase, post-PCR procedures, or restriction enzymes are required. Other Advantages of pET100 TOPO vector include cleavable detection and purification tag. The map of this vector is shown in figure 6. The flesh blunt-end PCR product was cloned directionally, at greater than 90% efficiency, into pET100 (obtained from Invitrogen) containing six histidine codons as a tag at the N-terminus in order to facilitate purification, and the *Mj0973* coding sequence was inserted downstream of the T7 promoter. The recombinant gene was expressed in *E. coli* strain BL21 (DE3) (obtained from Novagen) using the TOPO system (Invitrogen). This strain was grown in Luria Broth (LB) medium containing 50µg/ml ampicillin.

Expression and Purification of the Recombinant Enzyme

The transformed *E. coli* strain BL21 (DE3) was grown to an optical density of 0.6-0.7 (as measured using an eppendorf BioPhotometer plus), followed by induction with Isopropyl-beta-D-thiogalactopyranoside (IPTG) at a final concentration of 1.0 mM. After 6 h of induction at 30 ºC with shaking, cells were harvested by centrifugation at 4750 x g for 20 min at 4 ºC using a Beckman Coulter Allegra® X-15R centrifuge. The resulting cell pellet was resuspended in a buffer containing 30 mM Tris-HCl (pH 8.0) and 200 mM NaCl. The cell suspension was passed through a French Press four times at a pressure of 12,000 psi, resulting in cell lysis. The resulting cell lysate was centrifuged at 25,000 x g for 20 min to pellet the cell debris. The supernatant was passed through a 0.45 micron filter, and the filtrate was loaded onto a Ni^{2+} affinity column (HisTrap^{TM} HP purchased from GE Healthcare) anchored to a BioRad BioLogic LP Liquid Chromatography System that was pre-equilibrated with 20 ml Binding buffer (30 mM

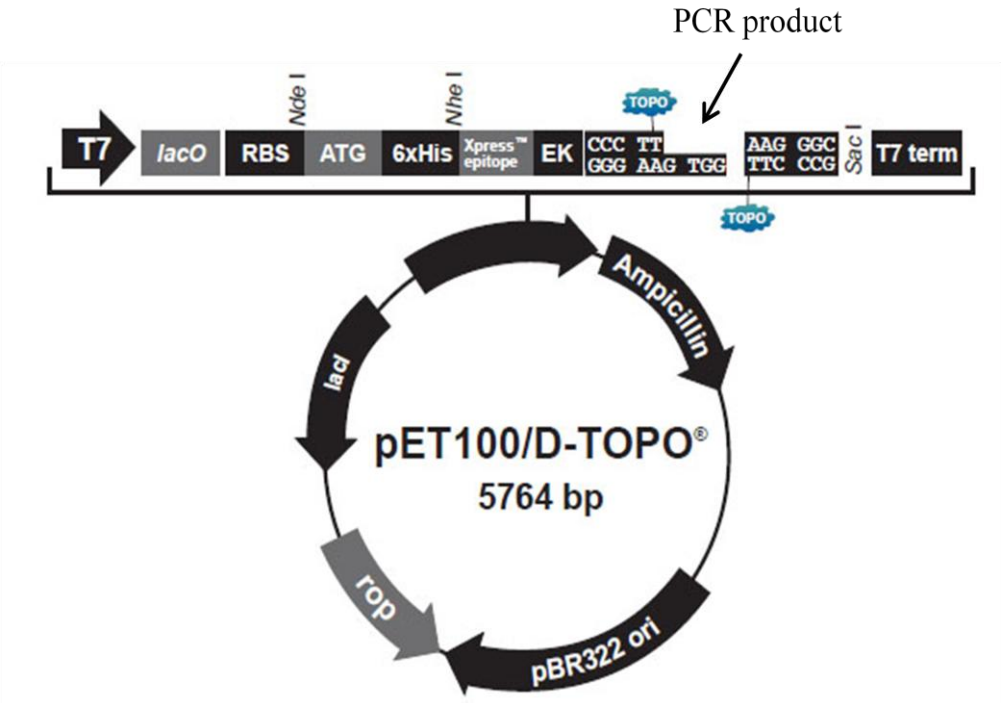

Figure 6. pET 100/D-TOPO vector map. pET 100/D-TOPO vector consists of total 5764 nucleotides. The contents for this vector include followings: T7 promoter: bases 209-225, T7promoter priming site: bases 209-228, lac operator (lacO): bases 228-252, Ribosome binding site (RBS): bases 282-288, Initiation ATG: bases 297-299, Polyhistidine (6xHis) region: bases 309-326, EK recognition site: bases 375-389, TOPO recognition site 1: bases 396-400, Overhang: bases 401-404, TOPO recognition site 2: bases 405-409, T7 reverse priming site: bases 466-485, T7 transcription termination region: bases 427-555, *bla* promoter: bases 856-954, Ampicillin resistance gene: bases 955-1815, pBR322 origin: bases 2022-2757, *ROP* ORF: bases 3001-3192, and *lacI* ORF: bases 4507-5595. This figure is adopted from http://tools.invitrogen.com/content/sfs/vectors/pet100dtopo_map.pdf

Tris-HCl (pH 8.0), 500 mM NaCl). After washing the column with Binding buffer containing 15 mM imidazole to remove nonspecifically bound proteins, the recombinant protein was eluted from the column with a 60 ml linear gradient that ranged from 15 - 250 mM imidazole in elution buffer containing 30 mM Tris-HCl (pH 8.0) and 500 mM NaCl, at a flow rate of 1 ml/min. Fractions were collected at an imidazole concentration of approximately 150 mM and concentrated using a Millipore Amicon Ultra-15 Centrifugal filter. The imidazole and salt in the concentrated protein was eliminated by exchanging buffers twice, each time with 10 ml of a 30 mM Tris-HCl (pH 8.0) and 100 mM Na_2SO_4 buffer, and the protein was retrieved in 1-2 ml of the same buffer. The concentrated and desalted protein was diluted to 10 ml with a solution containing 50 mM Glycine-KOH, pH 9.8 (Buffer A). This solution was loaded onto an anion exchange column (HiTrap Q HP purchased from GE Healthcare) attached to a BioRad BioLogic LP Liquid Chromatography System that was pre-equilibrated with 25 ml Buffer A. The column was washed with 30 ml of Buffer A, and recombinant protein was eluted by sequential addition of 2.5 ml each of 100, 200, 300, 400, 500, 600, 700, 800 and 1000 mM NaCl containing 50 mM Glycine-KOH, pH 9.8. Fractions at a NaCl concentration of 700 mM, 800 mM, and 1000 mM were collected and concentrated using a Millipore Amicon Ultra-15 Centrifugal filter. The concentrated protein was desalted by exchanging buffers twice, each time with 10 ml of a 30 mM Tris-HCl (pH 8.0) and 100 mM Na_2SO_4 buffer, and the desalted protein was stored in 1 ml of the same buffer. The purity of the recombinant protein was confirmed by SDS-PAGE. Protein concentrations were measured by UV-Vis analysis on a SHIMADZU UV-2450 UV-VIS spectrophotometer using the Bradford method [13] with bovine serum albumin as a standard. The typical yield was approximately 5 mg of protein from 1 L of *E. coli* culture.

Enzyme Assays

The APR and PAPR activities of the purified recombinant protein were measured in the presence of thioredoxin (Trx) and glutaredoxin (Grx) as electron donors. The 1 mL reaction mixture contained a final concentration of 5 µM recombinant protein, 100 mM Tris-HCl (pH 8.5), 1 mM EDTA (pH 8.0), 300 µM NADPH (Sigma-N 1630), 7 mM GSH or 1 mM Trx, 45 nM Glutathione Reductase (Sigma-G3664-100UN) or 1 µM NTR, and 0.1 - 3 µM APS (Sigma-N 1630) or 1-60 µM PAPS (Sigma-A 1651). The Tris-HCl buffer was replaced with 50 mM MES, 50 mM HEPES, and 50 mM Tricine for the pH dependence of the reactions studied. The assay was initiated by the addition of APS or PAPS at 30 ºC. The amount of NADPH oxidized was measured by monitoring the decrease in absorbance at 340 nm using a SHIMADZU UV-2450 UV-VIS spectrophotometer. The initial velocity rates were calculated based on an absorption coefficient value of 6.22 mM^{-1} cm^{-1} for NADPH at 340 nm. The mean data were obtained by three independent replicates. Kinetic constants were calculated using the Lineweaver-Burk method.

Ultraviolet-Visible Spectrum of Purified Enzyme

A solution of the recombinant enzyme in 30 mM Tris-HCl (pH 8.0) and 100 mM Na_2SO_4 buffer was scanned using a SHIMADZU UV-2450 UV-VIS spectrophotometer. The full spectrum wavelength range was set between 200 nm and 600 nm.

CHAPTER THREE

Results

Sequence Analysis of Homology to APR or PAPR

In order to predict whether Mj0973 possesses sequence homology with other APRs or PAPRs, a neighbor-joining tree was constructed and an amino acid sequence alignment with known APRs and PAPRs from both eukaryotes and prokaryotes was performed. Although amino acid sequence alignment showed relatively low homology with both APRs and PAPRs (Fig.8), Mj0973 possesses sequence similarity with two highly-conserved, key regions in APRs, CCXXRKXXPL(Conserved-Region 1) and SXGCXXCT (Conserved-Region 2) [14]. In addition, the dendrogram in Figure 7 indicates that Mj0973 is more closely related to APRs. Thus, the analyses resulting from the neighbor-joining tree and the amino acid sequence alignment suggest that Mj0973 is more likely an APR than a PAPR.

Mj0973 possesses several unique characteristics within the conserved regions mentioned in the previous paragraph. In most known APRs, the four cysteine residues (marked with dots in Fig. 8A) in Conserved-Regions 1 and 2 appear to be responsible for the binding of a [4Fe-4S] cluster [14, 15]. The cysteine residues in these conserved regions, thus, are known to be both structurally and catalytically important. While Mj0973 contains four cysteine residues in Conserved-Regions 1 and 2 (Cys^{259}, Cys^{263}, Cys^{345}, and Cys^{348}), only three of these residues are located in conserved cysteine positions. Cys^{263} (marked with an arrow in Fig. 8A) in Conserved-Region 1 is located three residues away from a conserved cysteine position of known APRs (CXXXCKXXPL instead of CCXXRKXXPL).

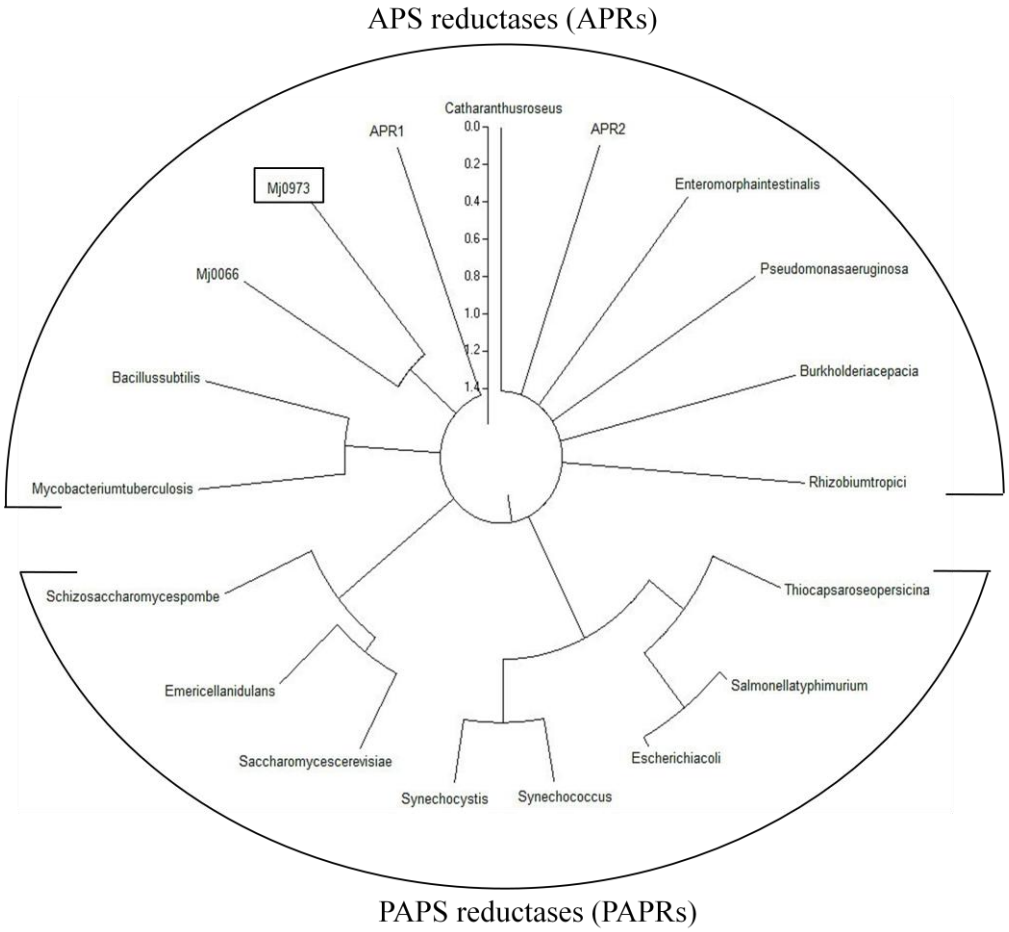

Figure 7. The neighbor-joining tree of APRs and PAPRs sequences. The dendrogram shows the amino acid sequence relationship between Mj0973 and various known APRs and PAPRs. The sequences were aligned using BioEdit, and the tree was constructed with MEGA version 4.0. The sequences were obtained from the NCBI sequence databases.

In addition, it was observed that Conserved-Region 2 of Mj0973 possesses a cysteine-proline (CP) motif (marked with an arrow in Fig 8A) which has been identified in other proteins as a potential heme binding site [16]. Thus, the presence of these sequence variations within Conserved-Regions 1 and 2 indicate that Mj0973 could possess different structural characteristics from other APRs.

(A)

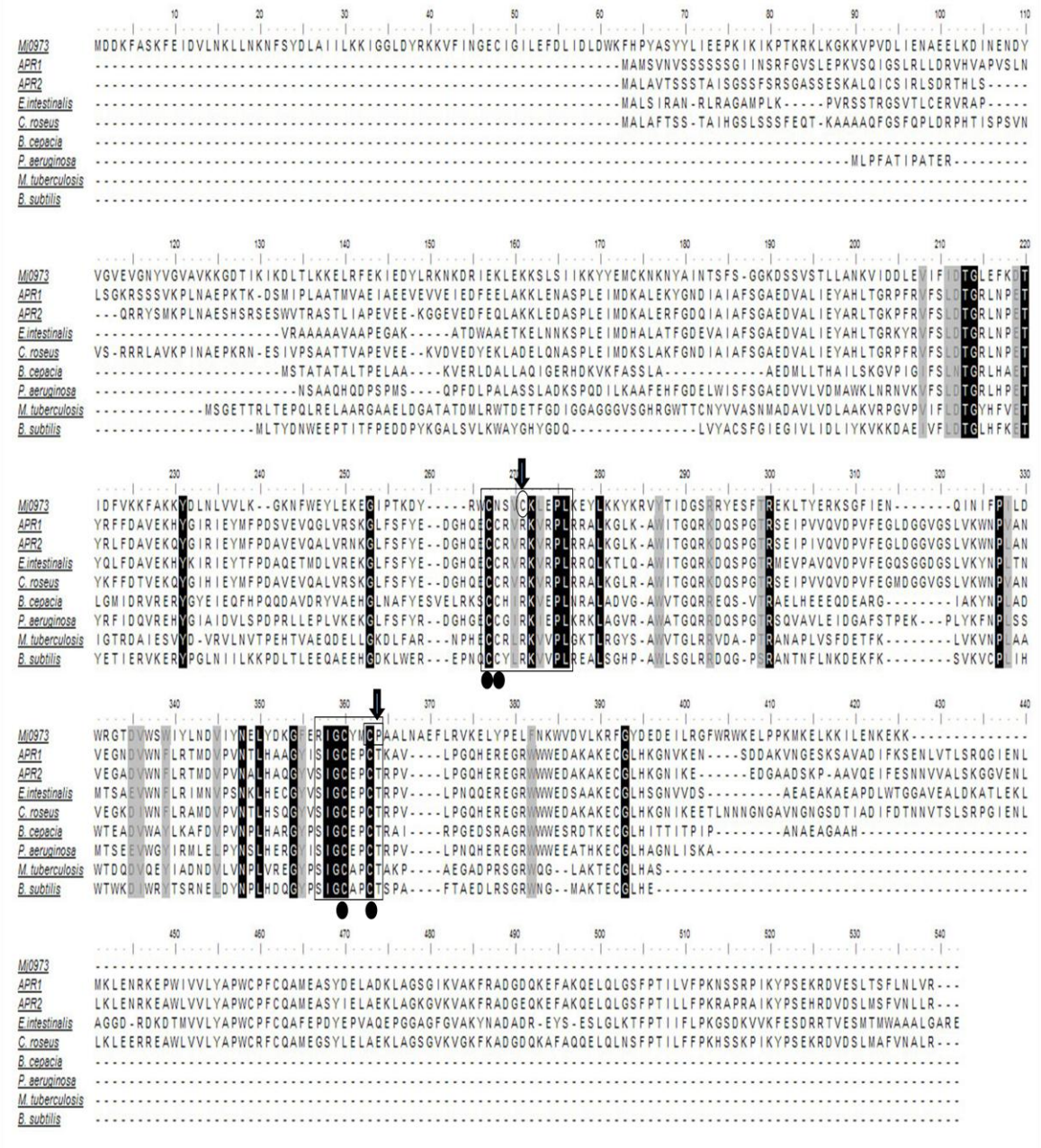
Mi0973
APR1
APR2
E.intestinalis
C. roseus
B. cepacia
P. aeruginosa
M. tuberculosis
B. subtilis

(B)

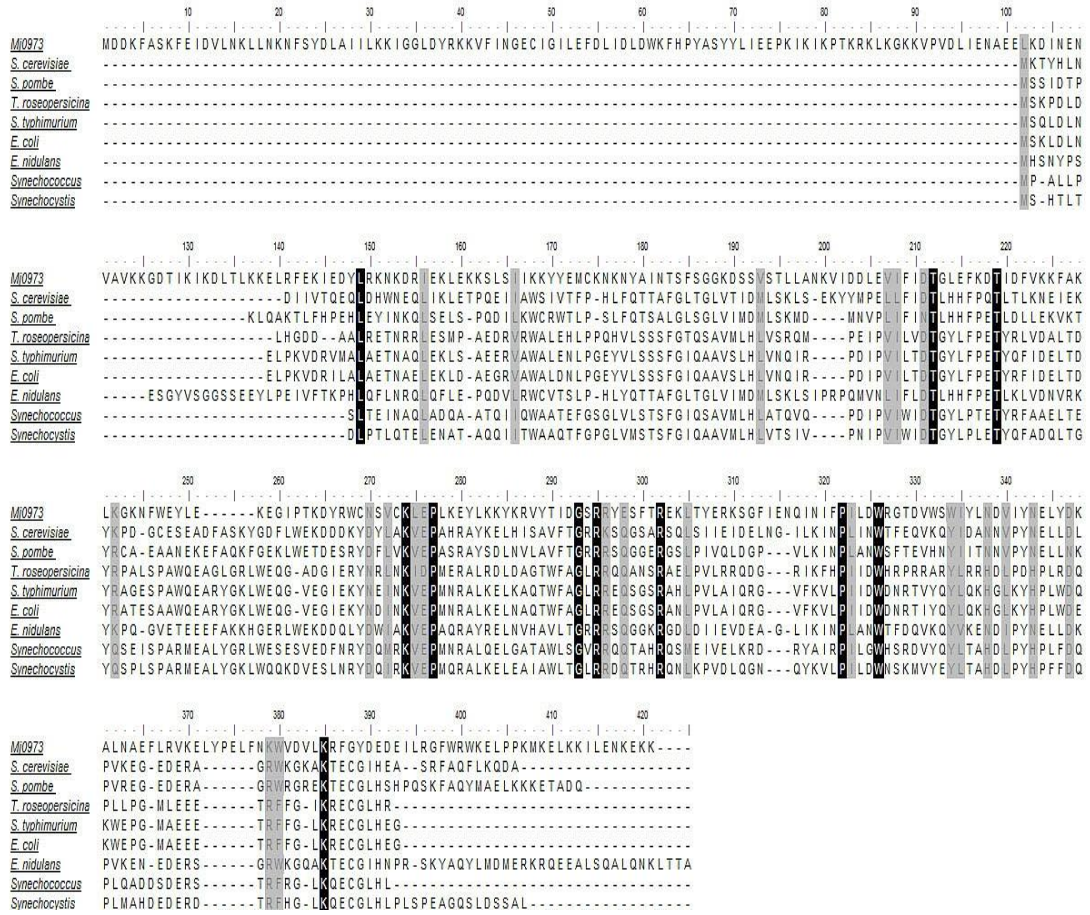

Figure 8. Multiple sequence alignment of Mj0973 with known APRs and PAPRs. Sequences were obtained from the NCBI sequence databases. Alignment was performed with BioEdit. (A) Sequence alignment of Mj0973 and APR homologs. (B) equence alignment of Mj0973 and PAPR homologs.

Docking Results from Homologous Structure of Mj0973 with Substrates, APS and PAPS

In order to study the predicted binding of Mj0973 with APS and PAPS, enzyme-substrate docking experiments were simulated via *in silico* modeling. Since no crystal structure of Mj0973 was available, substrates were docked with a homology modeling-based structure of Mj0973 obtained from SWISS-MODEL (Fig.9). The model consists mainly of alpha helixes (nine alpha helixes and three beta sheets).

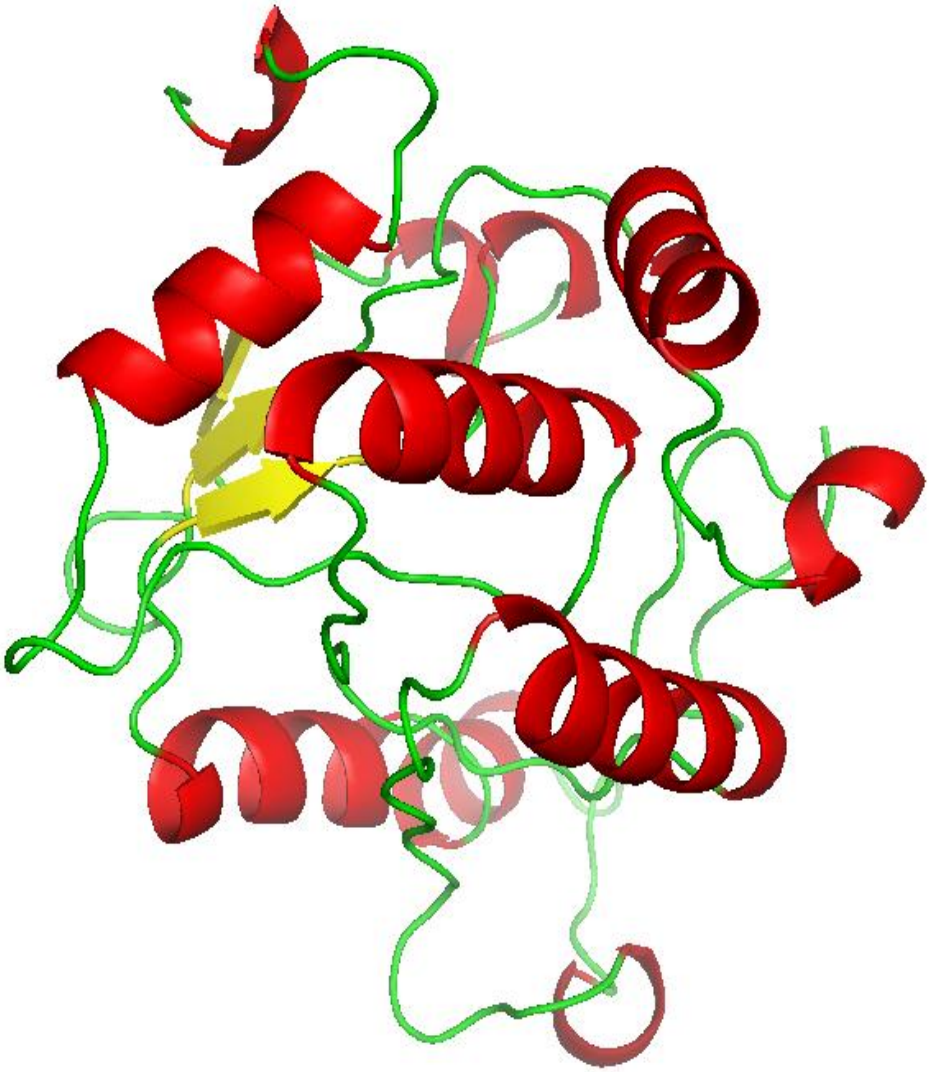

Figure 9. 3-D structure of the homologous modeling-based model of Mj0973. The alpha helix is shown in red, the beta sheet is shown in yellow, and the loop is shown in yellow.

The homologous modeling-based model of Mj0973 was then compared with the 3-D structures of other known APRs (shown in Fig. 10A, B, and C) to investigate any structural similarities. The observation of structure comparison indicated that they consist mainly of alpha helixes like the homologous modeling-based model of Mj0973. This similar secondary protein structure thus demonstrates that Mj0973 is likely to share the specific geometric shape of other known APRs caused by intramolecular and intermolecular hydrogen bonding of amino groups.

(A)

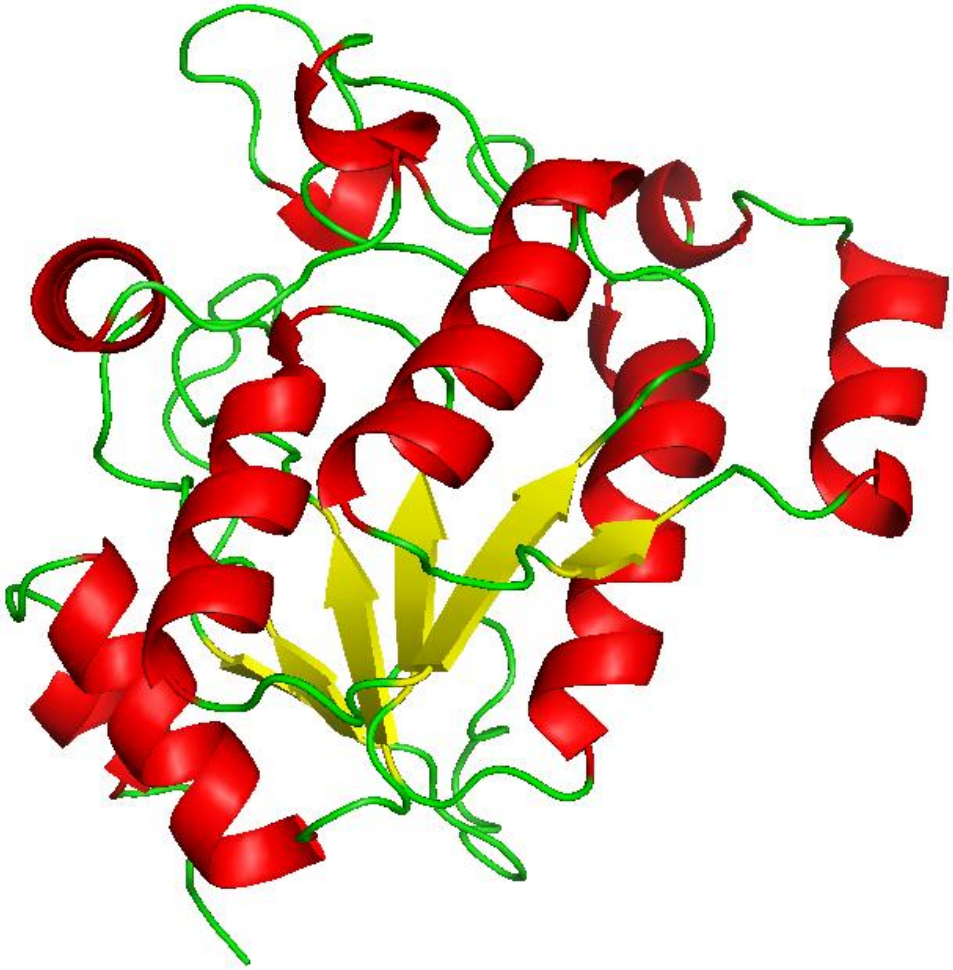

(B)

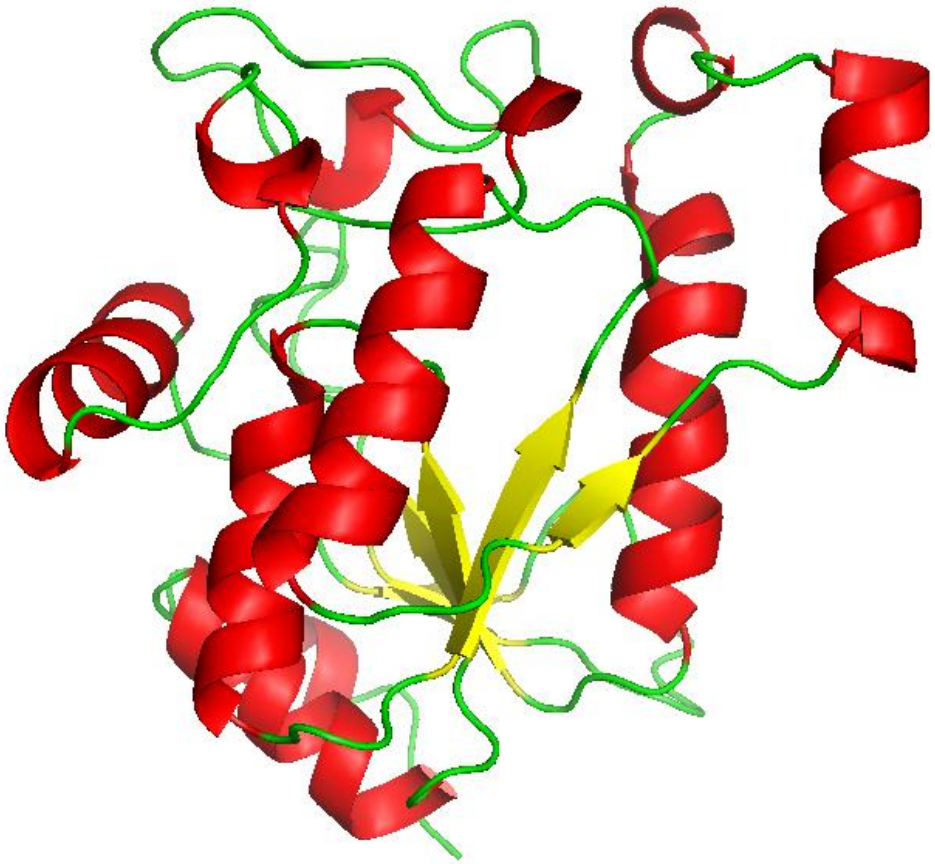

(C)

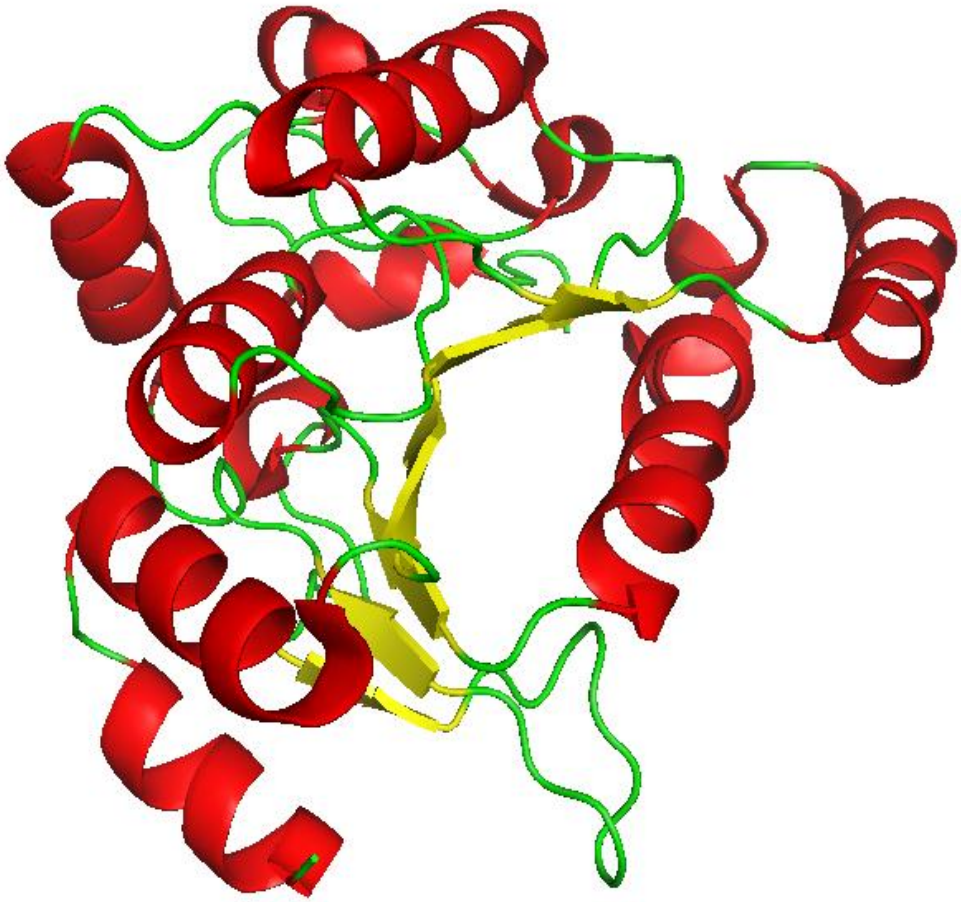

Figure 10. 3-D structure of known APRs. The alpha helix is shown in red, the beta sheet is shown in yellow, and the loop is shown in yellow. (A) 3-D structure of APR2 (*Cattharanthus roseus*). (B) 3-D structure of PpAPR (*physcomitrella patens*). (C) 3-D structure of PaAPR (*Pseudomonas aeruginosa*)

In homologous modeling-based model model of Mj0973, the four cysteines in Conserved-Regions 1 and 2 (Cys^{259}, Cys^{263}, Cys^{345}, and Cys^{348}) form a binding pocket, as shown in Figure 11. Thus, the binding energy and proximity between these conserved regions and the substrates were investigated through enzyme-substrate docking experiments.

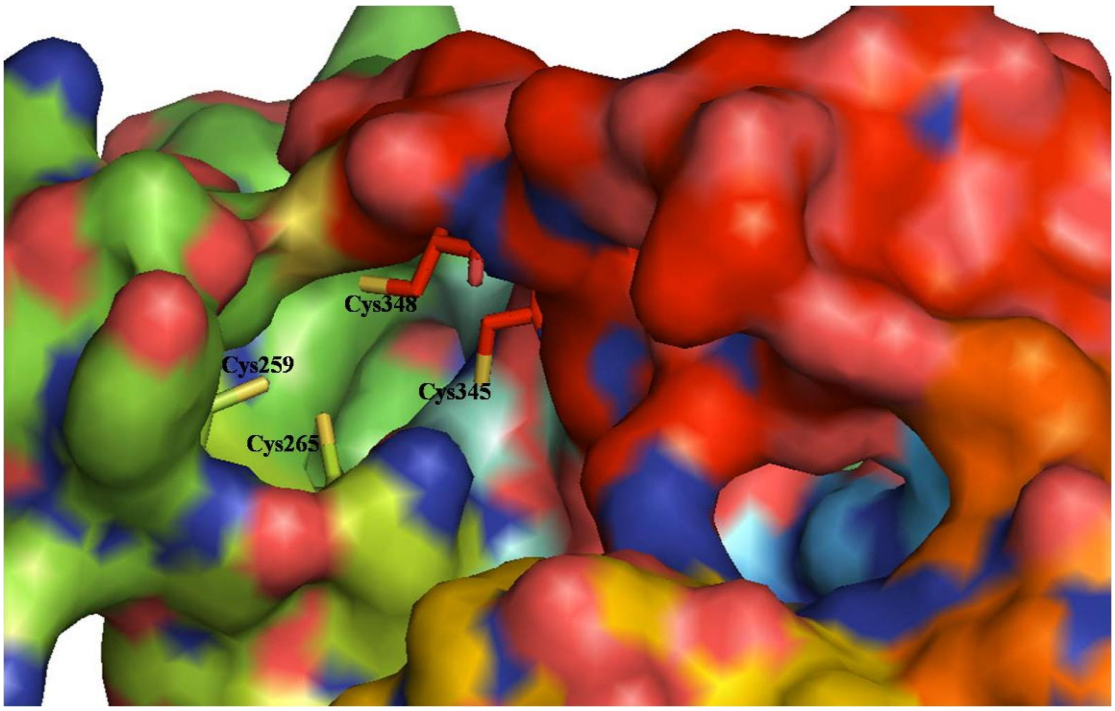

Figure 11. Molecular surface map of the homologous modeling-based model of Mj0973. Conserved binding pocket is shown with Cys^{259}, Cys^{263}, Cys^{345}, and Cys^{348} represented by stick models.

The results of the docking experiments are shown in Table 1 and Figure 12. For APS, the lowest predicted binding energy was -6.02 kcal/mol. Three hydrogen bond interactions occurred between the sulfate oxygen of APS and the amine hydrogen of Thr^{253} (2.913 Å), the sulfate oxygen of APS and the amine hydrogen of Asn^{260} (2.812 Å), and the furan ring oxygen of APS and the thiol side chain of Cys^{348} (2.701 Å). For PAPS, the lowest predicted binding energy was -4.53 kcal/mol. Two hydrogen bond

interactions occurred between the sulfate oxygen of PAPS and the hydroxyl side chain of Thr^{253} (2.015 Å), and the phosphate oxygen of PAPS and the hydroxyl hydrogen of Tyr^{256} (2.9 Å). The docking results showed that APS possesses a lower predicted binding energy and more hydrogen bonding interactions than PAPS. Since the Cys^{348} residue within the binding pocket forms a hydrogen bond with APS, the data indicates that APS binds in close proximity to the binding pocket of the target protein. As shown in Figure 12, the sulfate moiety of APS is oriented toward the interior of the binding pocket, indicating a higher probability of bond cleavage. Therefore, our docking study suggests that Mj0973 is more likely to reduce APS than PAPS.

Table 1. The best docking results of suggested compounds.

Substrate	Ntor	ΔG_{AD4} (kcal/mol)	RMSD (Å)	H-bonding interaction	H-bond distance (Å)
APS	6	-6.02	6.412	SO…HN(Thr253)	2.913
				SO…HN(Asn260)	2.812
				SH…OC(Cys348)	2.701
PAPS	6	-4.53	6.755	OH…OC(Thr253)	2.154
				OH…OH(Tyr256)	2.900

Ntor, the number of torsional degree of freedom in the compound; $\Delta G_{AD4,}$ the predicted free energy of binding from AutoDock4; RMSD, the root mean square difference in coordinates between the atoms and docked conformation

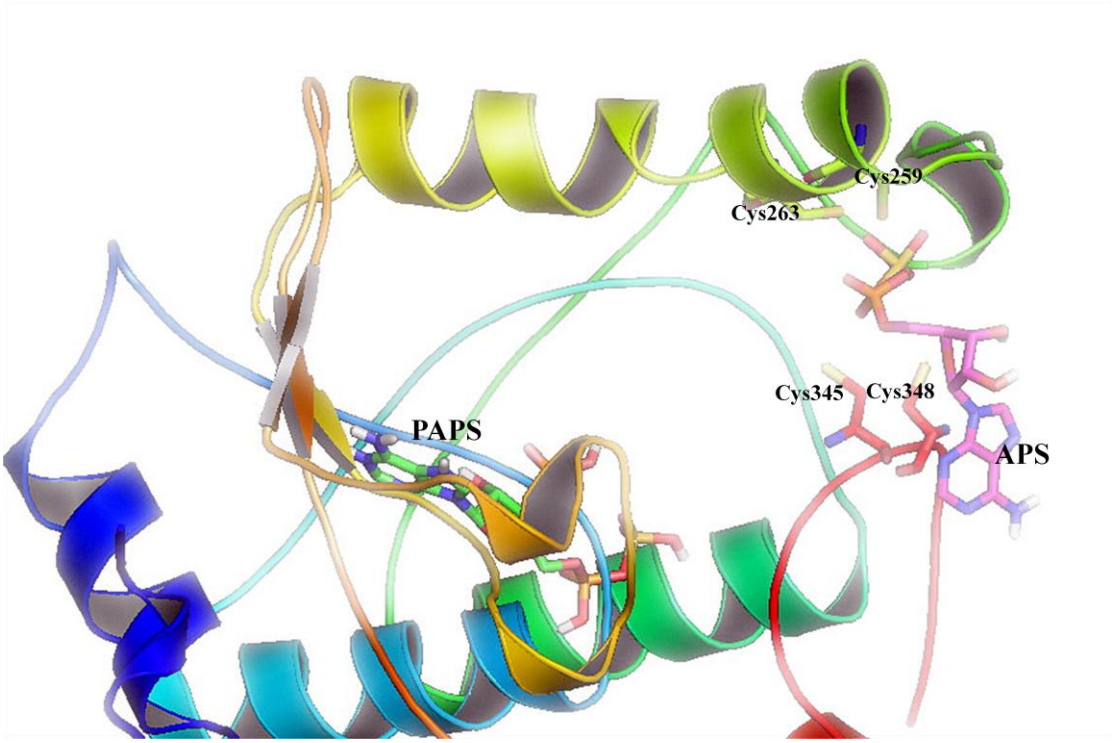

Figure 12. Docking simulation of the homologous modeling-based model of Mj0973 with APS and PAPS. A ribbon structure of the homologous modeling-based model of Mj0973 is shown. Cys^{259}, Cys^{263}, Cys^{345}, and Cys^{348} are represented by stick models. The sulfate moiety (yellow represents sulfur) of APS is docked in close proximity to the cysteine residues of the binding pocket.

Expression and Purification of rMj0973

At the time of this study, the putative gene product of ORF *Mj0973* had not been expressed and purified. The recombinant gene *Mj0973*, which contained a six-histidine tag, was expressed in an *E. coli* host system. The rMj0973 was initially purified using a Ni^{2+} affinity column. The purity of the protein was checked with SDS-PAGE analysis. However, SDS-PAGE analysis showed significant protein impurities (Fig.13 lane 1). In order to increase the purity of rMj0973, an anion exchange column was employed. SDS-PAGE analysis indicated that the re-purified recombinant protein showed a single Coomassie-staining band with a subunit molecular mass of approximately 49 kDa (Fig.13 lane 2), which is in accordance with the calculated mass of 48904 Da for rMj0973. Therefore, the results clearly demonstrate that the gene *Mj0973* can be successfully expressed in an *E. coli* host and the resulting protein purified to homogeneity without apparent dimer formation or proteolysis.

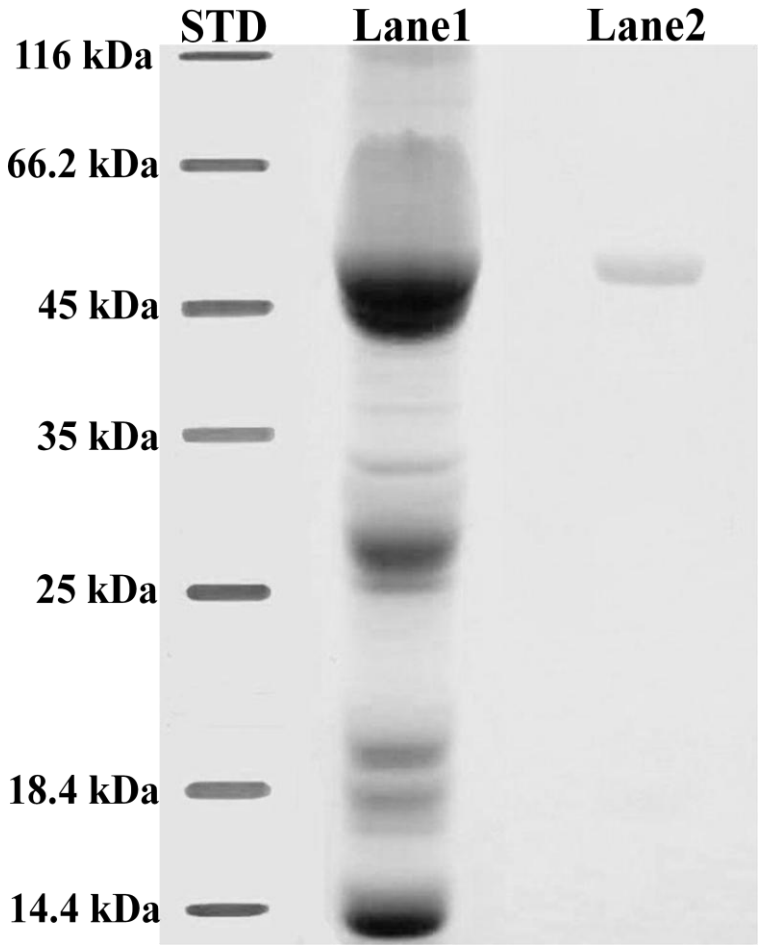

Figure 13. SDS-PAGE of purified rMj0973. STD, molecular size markers. Lane 1, Protein (36 µg) from the Ni^{2+} affinity column was loaded. Lane 2, Protein (7 µg) from anion exchange column was loaded. The gel was stained with Coomassie Brillant Blue R.

Substrate Specificity and Catalytic Constants of rMj0973

To determine the kinetic characteristics of rMj0973, a coupled enzyme assay was performed (Fig. 14). Here, the high energy reducing agent NADPH reduces NTR (NTR contains FAD and dithiol/disulfide couple redox active center), and subsequently the reduced NTR reduces the disulfide bond of Trx (i.e., oxidized form of Trx). The reduced Trx then is able to reduce Mj0973 by dithiol/disulfide couple reaction. Finally, the dithiol functional group of Mj0973 reduces the substrate APS by two electron donation.

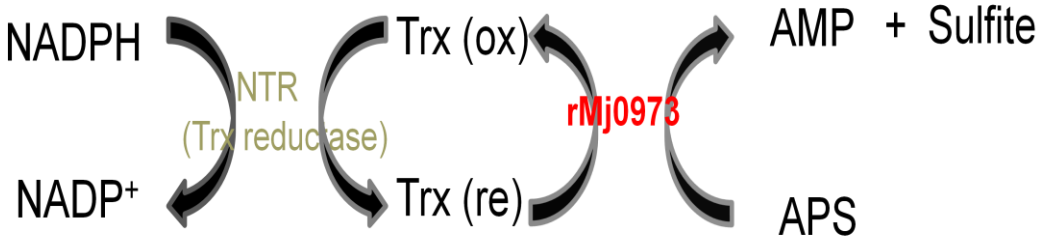

Figure 14. Dithiol/disulfide interchange reactions. Thioredoxin (Trx) reduce disulfide bonds in target proteins. Oxidized thioredoxin is reduced by thioredoxin reductase (NTR), which receives reducing equivalents from NADPH. The amount of NADPH oxidized was measured by monitoring the decrease in absorbance at 340nm.

The activity of purified rMj0973 was measured with varied concentrations of substrate (either APS or PAPS) and with saturating concentrations of an electron donor. In these assays, either glutaredoxin (Grx) or thioredoxin (Trx) was utilized as the electron donor, as described in previous APR and PAPR studies [2]. The data gleaned from the kinetics give a good fit into Michaelis-Menton equation (Fig. 15), and the Lineweaver-Burk method was used to visualize kinetic parameters (i.e., Km and Vmax) (Fig. 16).

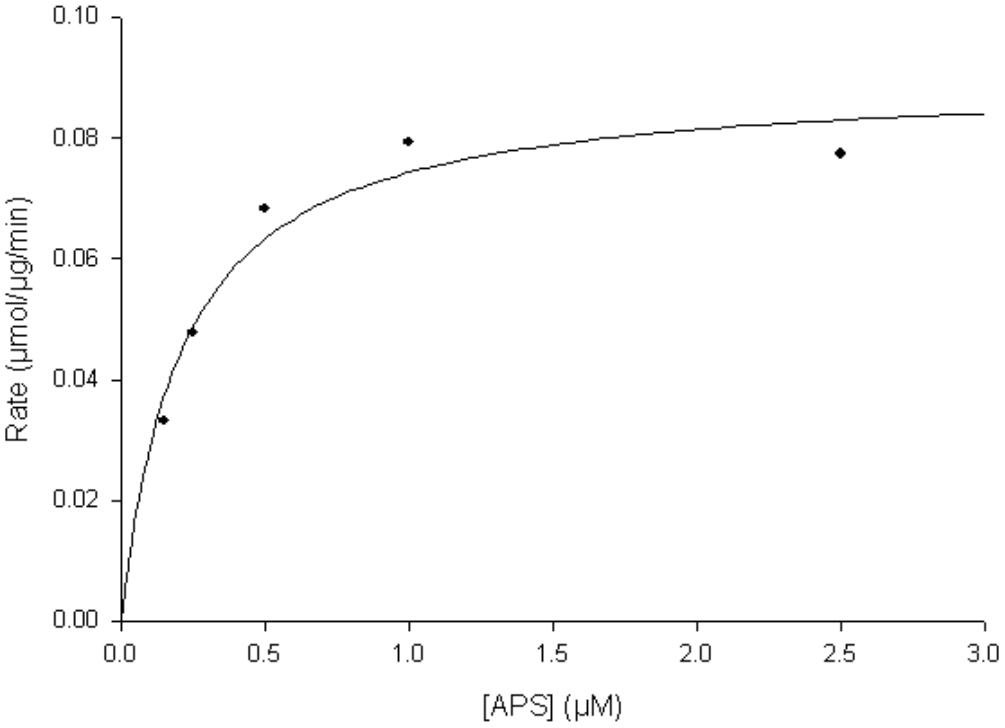

Figure 15. Michaelis-Menten plot.

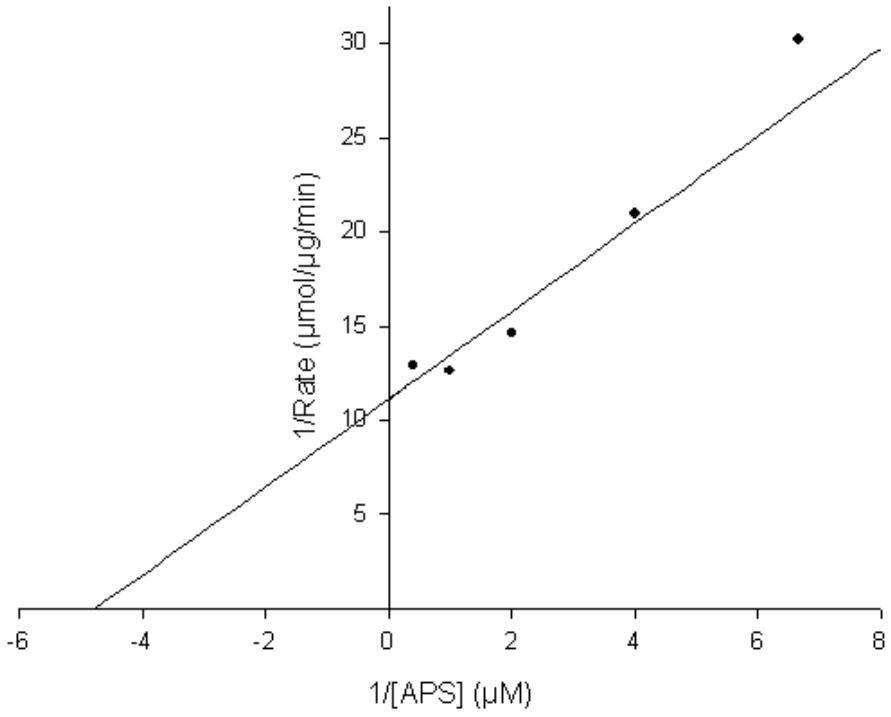

Figure 16. A double-reciprocal (Lineweaver-Burk) plot.

The K_m and V_{max} values of purified recombinant Mj0973 for APS were 0.29 μM and 0.079μMmg^{-1}min^{-1}, respectively. From this, a k_{cat} of 0.0869s^{-1} and a catalytic efficiency (k_{cat}/K_m) of 299,655M^{-1}s^{-1} were calculated. However, rMj0973 did not show any significant activity when PAPS was utilized as a substrate in combination with either Trx or Grx. The data are summarized in Table 2. These results indicate that rMj0973 possesses the ability to reduce APS, but is unable to reduce PAPS.

Table 2. Kinetic parameters of MjAPR

Substrate	Electron donor	K_m(μM)	V_{max}(μmol/mg·min)	k_{cat}(1/s)	k_{cat}/K_m(1/M·s)
APS	Trx	0.29	0.079	0.0869	299,655
APS	Grx	None*	None	None	None
PAPS	Trx	None	None	None	None
PAPS	Grx	None	None	None	None

Recombinat Trx or Grx from *E.coli* was used as electron donor. None* indicates there was no detectable activity.

UV-Vis Analysis of rMj0973

In order to gather information on any cofactors utilized by rMj0973, a UV-visible spectrum was obtained for the purified protein. The result shows a shoulder around 400 nm and a marked maximum at 414 nm (Fig. 17). Exposure to air for 1 h had no effect on the spectrum, indicating that the cofactor was completely oxidized in the purified rMj0973. The addition of 0.2 mM potassium cyanide (KCN), a known heme protein inhibitor, shifted the maximum peak from 414 nm to 425 nm, as shown in Figure 17 with a dashed line. These results possibly indicate the presence of a heme cofactor in rMj0973.

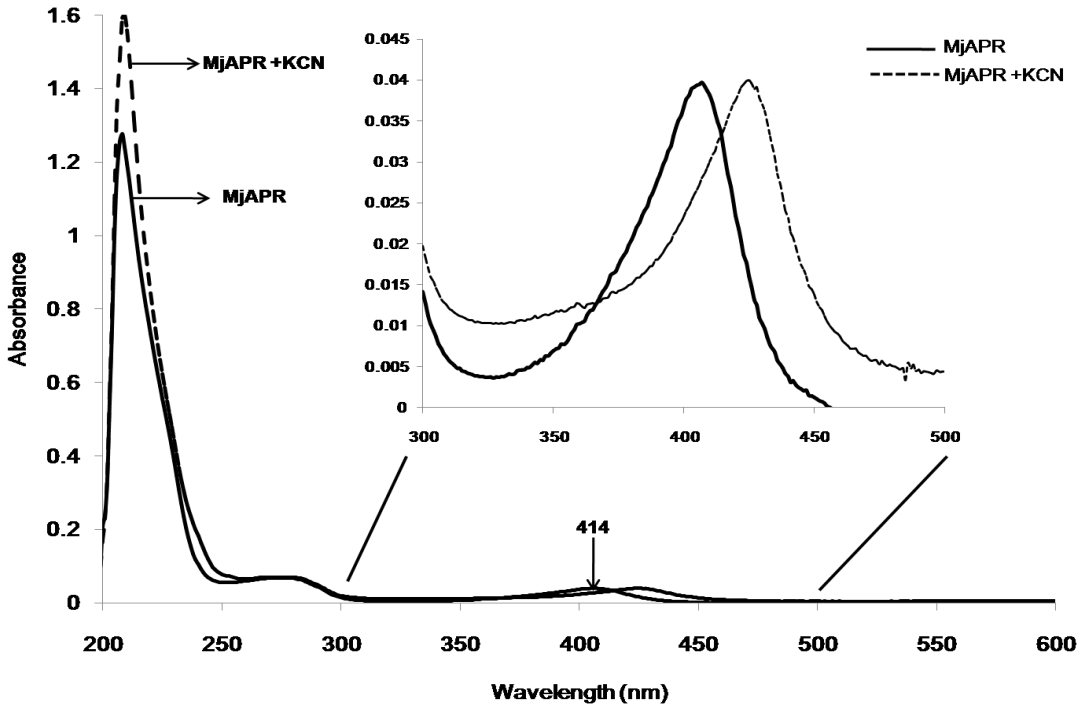

Figure 17. UV/vis spectrum analysis of MjAPR. Solid line indicates MjAPR and dashed line indicates MjAPR with KCN. A spectrophotometric shift accompanied the reaction of MjAPR (20 µM) with KCN (0.2 mM) in the presence of 30 mM Tris-HCl (pH 8.0) buffer with 100 mM Na_2SO_4. The blank cell containing 30 mM Tris-HCl (pH 8.0) buffer with 100 mM Na_2SO_4 was used as the reference cell.

CHAPTER FOUR

Discussion

Determination of MjAPR and an Interspecies Comparison of Kinetic Data

Our results provide the first convincing evidence that *M. jannaschii* reduces APS using a previously uncharacterized sulfonucleotide reductase. In our amino acid sequence alignment, Mj0973 showed relatively low homology with other APRs and PAPRs but was highly conserved in the key regions of APRs. In our phylogenetic analysis, the dendrogram clearly clustered Mj0973 with other APRs from eukaryotes and prokaryotes. In addition, the docking simulation of APS with the homology modeling-based structure of Mj0973 resulted in close substrate binding proximity to the conserved binding pocket with lower binding energy than PAPS. Therefore, the enzyme is expected to catalyze the reduction of APS to sulfite. In accordance with the above computational analyses, our kinetic study revealed that the Mj0973 indeed possesses APR activity. The kinetic study also revealed that the activity of Mj0973 was dependent on Trx. This is not surprising because previous studies on APRs from a wide range of taxonomies, such as plant (*Arabidopsis thaliana*), moss (*Physcomitrella patens*), and bacteria (*Pseudomonas aeruginosa*, *Pseudomonas putida*, and *Bacillus subtilis*) [2, 14-17] showed that these enzymes also utilize Trx as an electron donor. Thus, this study have revealed that the protein produced by the gene *Mj0973* acts as an APR mediated by Trx.

A comparison of our kinetic data with other APRs indicated that there may be a relationship between the catalytic efficiency of an APR and the phylogenetic classification of the source organism. As shown in Table 3, an analysis of the kinetic

data reported in previous APRs studies revealed that catalytic efficiency of APRs in both plant (AtAPR) and moss (PpAPR) were 1200-fold higher than APR in bacteria (BsAPR), indicating that the catalytic efficiency of an APR increases with the complexity of its source organism [1, 17]. Therefore, the catalytic efficiency of MjAPR from archaea was expected to be between the efficiencies of eukaryotic APRs and prokaryotic APRs. Indeed, when the catalytic efficiency of MjAPR was compared to the APR in a plant (AtAPR), moss (PpAPR), and bacterium (BsAPR), it was found that MjAPR could reduce APS 58-fold more efficiently than BsAPR but 21-fold less efficiently than both PpAPR and AtAPR (Table 3). Since *M. jannaschii* is in-between eukaryotes and prokaryotes in the phylogenetic tree, this observation seems to suggest that the efficiency of APS metabolism could be related to the phylogenetic classification of the source organism. Further investigation is needed in this area to determine if any relationship exists.

Table 3. Kinetic constants of various APRs

	K_m(μM)	k_{cat}(1/s)	k_{cat}/ K_m(1/M.s)	Ref (#)
AtAPR2	6	37.5	6,250,000	[1]
PpAPR	6	37.5	6,250,000	[1]
MjAPR	0.29	0.0869	299655	
BsAPR	28.7	0.149	5200	[17]
PpAPR-B	50	0.176	3520	[1]

Activities of AtAPR2 (*Arabidopsis thaliana*), PpAPR (*Physcomitrella patens*), BsAPR (*Bacillus subtilis*) and PpAPR-B (PpAPR without FeS) were measured with Trx as the electron donor.

Cofactor Analysis

This study have shown strong evidence that MjAPR is a novel APR which lacks a [4Fe-4S] cluster. As mentioned previously, most known APRs possess two conserved motifs (CCXXRKXXPL and SXGCXXCT). The cysteine residues found in these motifs are known to be ligands for a [4Fe-4S] cluster [14, 15] which is involved in the reduction of APS [1, 15, 16, 18]. However, our homology sequence analysis revealed that the arrangement of cysteines within Conserved-Region1 of MjAPR (Cys^{259}, Cys^{263}) deviates from the conserved motif of most known APRs. Since these cysteines are implicated in the binding of the [4Fe-4S] cluster, this sequence variation is expected to cause a change in tertiary structure which may prevent the binding of a [4Fe-4S] cluster. The presence of a [4Fe-4S] cluster was investigated by UV-vis absorbance spectrum analysis. The UV-vis absorbance spectrum of a protein containing a single [4Fe-4S] cluster typically shows a broad peak with a maximum at 386 nm [14, 19]. The UV-vis spectrum of MjAPR does not possess these characteristics. Therefore, it can be tentatively concluded that MjAPR lacks a [4Fe-4S] cluster.

Although MjAPR seems to lack an iron-sulfur cluster, our results still indicate the presence of a cofactor. A previous study demonstrated that the lack of a cofactor significantly impairs the enzyme's affinity and catalytic ability [1]. For instance, PpAPR without an iron-sulfur cluster (PpAPR-B) is 1770-fold less efficient than PpAPR with an iron-sulfur cluster [1]. If MjAPR lacks a cofactor, then its catalytic efficiency is expected to be relatively low, like that of PpAPR-B. However, a comparison of the catalytic efficiencies from MjAPR and PpAPR-B (Table 3) revealed that MjAPR is 85-fold more efficient than PpAPR-B. This suggests that MjAPR is likely to possess a catalytically-involved cofactor. Moreover, the apparent peak at 414 nm from our UV-vis spectrum strongly evinces the presence of a cofactor. Since SDS-PAGE analysis of the

purified protein clearly showed a single band, this cofactor should be from MjAPR, not protein contamination.

Possible Presence of a Heme Cofactor

The results indicate the presence of a heme cofactor in MjAPR. From the homology sequence analysis, it was observed that MjAPR, unlike other APRs, possesses a CP motif (a dipeptide cysteine-proline) within Conserved-Region 2. CP motifs are associated with heme-mediated regulation [20] and it has previously been demonstrated that a peptide containing a single CP motif is capable of binding a heme group [21]. In fact, a previous study discovered a heme group within Iron Regulatory Protein (IRR), a bacterial protein which, like MjAPR, contains only one CP motif [22]. Domain structures of the heme-regulated protein IRR, and 3-D structure of the homologous modeling-based model of IRR are shown in Figure 18 and 19, respectively. However, the obtained homologous modeling-based model of IRR from SWISS-MODEL provides only modeled residue range of 36 to 163. Therefore, unfortunately, the heme-binding site, which is expected to be located around residue 29 (cystein) and 30 (proline), was not able to be investigated.

Figure 18. Domain structures of the heme-regulated protein IRR. IRR contains a single heme-regulated motif (HRM). (adopted from [22])

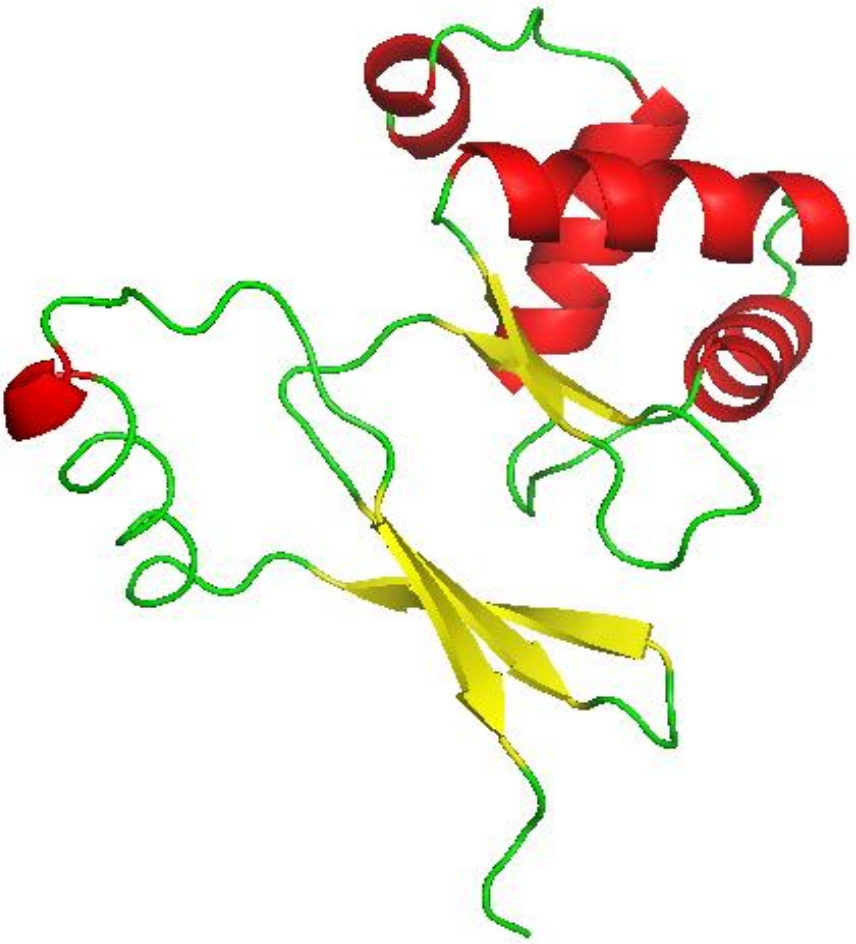

Figure 19. 3-D structure of the homologous modeling-based model of IRR from *Bradyrhizobium japonicum*. Modeled residue range is from 36 to 163. The alpha helix is shown in red, the beta sheet is shown in yellow, and the loop is shown in yellow.

Furthermore, our UV-Vis absorbance spectrum showed a shoulder around 400 nm and a marked maximum at 414 nm, which are characteristic of a heme cofactor [23, 24]. When KCN was added, the marked maximum shifted to 425 nm. Previous studies have shown that many known heme proteins undergo a similar spectral shift in the presence of KCN [25-28]. Therefore, our findings suggest that MjAPR contains a heme cofactor which is most likely bound to Cys^{348}, a part of the CP motif. Future studies should be focused on the crystal structure and mutational analysis of MjAPR in order to confirm the presence of a heme group and define its function.

Sulfate Reduction Pathway

Our discovery of an APR in *M. jannaschii* strongly indicates the existence of the sulfate reduction pathway in this organism. However, in order to confidently propose such a pathway in a methanogen, two issues should be addressed: (i) What is the sulfate source? and (ii) How can the organism utilize the sulfate reduction pathway without permitting sulfite-inhibition of methanogenesis? As previously noted, *M. jannaschii* resides in sulfide-rich deep-sea hydrothermal vents [5]. While sulfide is the predominant sulfur compound, there is evidence that more oxidized sulfur compounds, such as sulfate, are also present in this environment. Studies have found that when cold seawater encounters the 350 ºC vent fluid, sulfide reacts with oxygen in the seawater, providing a sulfate source [5, 29, 30]. Although necessary, mere presence of a sulfate source does not imply the existence of a sulfate reduction pathway in this methanogenic archeon. Since an intermediate of the sulfate reduction pathway, sulfite, is a potent inhibitor of methanogenesis, these two metabolic processes are seemingly incompatible. However, a possible resolution for the conflict between sulfate reduction and methanogenesis was provided by the discovery of coenzyme F_{420} dependent sulfite reductase, an enzyme in

M. jannaschii that catalyzes the reduction of sulfite to sulfide without inhibiting methanogenesis [5]. Therefore, the presence of sulfate in this environment, the existence of coenzyme F_{420} dependent sulfite reductase, and our discovery of MjAPR strongly indicates the presence of a sulfate-reduction pathway in *M. jannaschii*. In order to complete the map of the sulfate reduction pathway in *M. jannaschii*, future investigations should focus on the discovery of other enzymes involved in this pathway (e.g. ATP sulfurylase, APS kinase, PAPR, etc).

CHAPTER FIVE

Conclusions and Future Directions

Here the first discovery of an APR in the Methanarcheon , *M. jannaschii* was reported. The open reading frame (ORF) *Mj0973* in the genome of *M. jannaschii* was successfully expressed and purified. Then, its substrate specificity and catalytic constants were measured. The results clearly show that *Mj0973* codes for an APR. Additionally, UV-vis absorbance spectrum analysis indicates that MjAPR possesses a heme cofactor. This discovery of MjAPR provides convincing evidence that the sulfate reduction pathway exists in methanarchea.

In order to complete the map of sulfate reduction pathway in *M. jannaschii*, further investigation should focus on discovery of other enzymes involved in this pathway (ATP sulfurylase, APS kinase, PAPR, etc). Since earlier studies have already noted that ORF Mj0066 possesses some sequence similarity to ATP sulfurylase and PAPR, Mj0066 appears to be an attractive subject for these investigations.

REFERENCES

[1] Kopriva S, Fritzemeier K, Wiedemann G, Reski R. The putative moss 3'-phosphoadenosine-5'-phosphosulfate reductase is a novel form of adenosine-5'-phosphosulfate reductase without an iron-sulfur cluster. J Biol Chem 2007;282:22930-22938.

[2] Bick JA, Dennis JJ, Zylstra GJ, Nowack J, Leustek T. Identification of a new class of 5'-adenylylsulfate (APS) reductases from sulfate-assimilating bacteria. J Bacteriol 2000;182:135-142.

[3] Lillig CH, Prior A, Schwenn JD, Aslund F, Ritz D, Vlamis-Gardikas A, Holmgren A. New thioredoxins and glutaredoxins as electron donors of 3'-phosphoadenylylsulfate reductase. J Biol Chem 1999;274:7695-7698.

[4] Kopriva S. Regulation of sulfate assimilation in Arabidopsis and beyond. Ann Bot 2006;97:479-495.

[5] Johnson EF, Mukhopadhyay B. A new type of sulfite reductase, a novel coenzyme F420-dependent enzyme, from the methanarchaeon Methanocaldococcus jannaschii. J Biol Chem 2005;280:38776-38786.

[6] Ronnow PH, Gunnarsson LA. Sulfide-Dependent Methane Production and Growth of a Thermophilic Methanogenic Bacterium. Appl Environ Microbiol 1981;42:580-584.

[7] Mazumder TK, Nishio N, Fukuzaki S, Nagai S. Effect of Sulfur-Containing Compounds on Growth of Methanosarcina barkeri in Defined Medium. Appl Environ Microbiol 1986;52:617-622.

[8] Wedzicha BL. Chemistry of sulphiting agents in food. Food Addit Contam 1992;9:449-459.

[9] Bult CJ, White O, Olsen GJ, Zhou L, Fleischmann RD, Sutton GG, Blake JA, FitzGerald LM, Clayton RA, Gocayne JD, Kerlavage AR, Dougherty BA, Tomb JF, Adams MD, Reich CI, Overbeek R, Kirkness EF, Weinstock KG, Merrick JM, Glodek A, Scott JL, Geoghagen NS, Venter JC. Complete genome sequence of the methanogenic archaeon, Methanococcus jannaschii. Science 1996;273:1058-1073.

[10] Tamura K DJ, Nei M & Kumar S. MEGA4: Molecular Evolutionary Genetics Analysis (MEGA) software version 4.0. Molecular Biology and Evolution 2007;24:1596-1599.

[11] Schuttelkopf AW, van Aalten DM. PRODRG: a tool for high-throughput crystallography of protein-ligand complexes. Acta Crystallogr D Biol Crystallogr 2004;60:1355-1363.

[12] Arnold K, Bordoli L, Kopp J, Schwede T. The SWISS-MODEL workspace: a web-based environment for protein structure homology modelling. Bioinformatics 2006;22:195-201.

[13] Bradford MM. A rapid and sensitive method for the quantitation of microgram quantities of protein utilizing the principle of protein-dye binding. Anal Biochem 1976;72:248-254.

[14] Kim SK, Rahman A, Bick JA, Conover RC, Johnson MK, Mason JT, Hirasawa M, Leustek T, Knaff DB. Properties of the cysteine residues and iron-sulfur cluster of the assimilatory 5'-adenylyl sulfate reductase from Pseudomonas aeruginosa. Biochemistry 2004;43:13478-13486.

[15] Kopriva S, Buchert T, Fritz G, Suter M, Benda R, Schunemann V, Koprivova A, Schurmann P, Trautwein AX, Kroneck PM, Brunold C. The presence of an iron-sulfur cluster in adenosine 5'-phosphosulfate reductase separates organisms utilizing adenosine 5'-phosphosulfate and phosphoadenosine 5'-phosphosulfate for sulfate assimilation. J Biol Chem 2002;277:21786-21791.

[16] Kopriva S, Koprivova A. Plant adenosine 5'-phosphosulphate reductase: the past, the present, and the future. J Exp Bot 2004;55:1775-1783.

[17] Berndt C, Lillig CH, Wollenberg M, Bill E, Mansilla MC, de Mendoza D, Seidler A, Schwenn JD. Characterization and reconstitution of a 4Fe-4S adenylyl sulfate/phosphoadenylyl sulfate reductase from Bacillus subtilis. J Biol Chem 2004;279:7850-7855.

[18] Kopriva S, Buchert T, Fritz G, Suter M, Weber M, Benda R, Schaller J, Feller U, Schurmann P, Schunemann V, Trautwein AX, Kroneck PM, Brunold C. Plant adenosine 5'-phosphosulfate reductase is a novel iron-sulfur protein. J Biol Chem 2001;276:42881-42886.

[19] Kim SK, Gomes V, Gao Y, Chandramouli K, Johnson MK, Knaff DB, Leustek T. The two-domain structure of 5'-adenylylsulfate (APS) reductase from Enteromorpha intestinalis is a requirement for efficient APS reductase activity. Biochemistry 2007;46:591-601.

[20] Ogawa K, Sun J, Taketani S, Nakajima O, Nishitani C, Sassa S, Hayashi N, Yamamoto M, Shibahara S, Fujita H, Igarashi K. Heme mediates derepression of Maf recognition element through direct binding to transcription repressor Bach1. EMBO J 2001;20:2835-2843.

[21] Zhang L, Guarente L. Heme binds to a short sequence that serves a regulatory function in diverse proteins. EMBO J 1995;14:313-320.

[22] Mense SM, Zhang L. Heme: a versatile signaling molecule controlling the activities of diverse regulators ranging from transcription factors to MAP kinases. Cell Res 2006;16:681-692.

[23] Kniemeyer O, Heider J. Ethylbenzene dehydrogenase, a novel hydrocarbon-oxidizing molybdenum/iron-sulfur/heme enzyme. J Biol Chem 2001;276:21381-21386.

[24] Kuzelova K, Mrhalova M, Hrkal Z. Kinetics of heme interaction with heme-binding proteins: the effect of heme aggregation state. Biochim Biophys Acta 1997;1336:497-501.

[25] Chen YR, Deterding LJ, Tomer KB, Mason RP. Nature of the inhibition of horseradish peroxidase and mitochondrial cytochrome c oxidase by cyanyl radical. Biochemistry 2000;39:4415-4422.

[26] Matsuno-Yagi A, Hatefi Y. Ubiquinol:cytochrome c oxidoreductase (complex III). Effect of inhibitors on cytochrome b reduction in submitochondrial particles and the role of ubiquinone in complex III. J Biol Chem 2001;276:19006-19011.

[27] Vasudevan G, McDonald MJ. Spectral demonstration of semihemoglobin formation during CN-hemin incorporation into human apohemoglobins. J Biol Chem 1997;272:517-524.

[28] Kimura S, Yamazaki I, Kitagawa T. Unusual low-frequency resonance Raman spectra of heme observed for hog intestinal peroxidase and its derivatives. Biochemistry 1981;20:4632-4638.

[29] Corliss JB, Dymond J, Gordon LI, Edmond JM, von Herzen RP, Ballard RD, Green K, Williams D, Bainbridge A, Crane K, van Andel TH. Submarine Thermal Sprirngs on the Galapagos Rift. Science 1979;203:1073-1083.

[30] Jannasch HW, Mottl MJ. Geomicrobiology of Deep-Sea Hydrothermal Vents. Science 1985;229:717-725.

[31] A Schmidt, and K Jäger. Open Questions about Sulfur Metabolism in Plants. Annual Review of Plant Physiology and Plant Molecular Biology 1992:43: 325-349